Effects of changes in stopping-power ratios with field size on electron beam relative output factors

G. G. Zhang
Carleton University, and NRC, Ottawa, Canada

D. W. O. Rogers[a)]
National Research Council of Canada, Ottawa, K1A 0R6 Canada

J. E. Cygler
Ottawa Regional Cancer Center, Ottawa, Canada

T. R. Mackie
University of Wisconsin, Madison, Wisconsin 53706

(Received 7 July 1997; accepted for publication 1 July 1998)

Stopping-power ratios are a function of field size and vary with accelerators. To investigate how these variations affect relative output factor measurements made using ion chambers for electron beams, especially for small fields, $(\overline{L}/\rho)^{\rm water}_{\rm air}$ is calculated using the Monte Carlo technique for different field sizes, beam energies, and accelerators and is compared to the data in TG-21 or TG-25, which are for mono-energetic broad beams. For very small field sizes defined by cutouts, if the change in $(\overline{L}/\rho)^{\rm water}_{\rm air}$ with $d_{\rm max}$ is ignored (i.e., TG-25 is not carefully followed), there is an overestimate of relative output factors by up to 3%. Ignoring the field-size effect on stopping-power ratio adds an additional overestimate of up to one-half percent, and using mono-energetic stopping-power ratio data instead of realistic beam data gives another error, but in the opposite direction, of up to 0.7%. Due to the cancellation of these latter two errors, following TG-25 with $(\overline{L}/\rho)^{\rm water}_{\rm air}$ data for broad mono-energetic beams will give the correct answer for the ROF measurement within 0.4% compared to using $(\overline{L}/\rho)^{\rm water}_{\rm air}$ data for which the field-size effect is considered for realistic electron beams. © *1998 American Association of Physicists in Medicine.*
[S0094-2405(98)01609-5]

I. INTRODUCTION

The output of electron beam accelerators is strongly dependent on the size of the field. Thus the measurement of outputs for different beam sizes is an important component of electron beam dosimetry in clinical practice. This is usually done as measurement of the output for a given field size relative to that of a reference field size, i.e., a relative output factor or ROF. Although people use different detectors for this kind of measurement, such as film[1,2] and silicon diode,[3] in most clinics ion chambers are used. To convert ionization to absorbed dose to water, a fundamental equation of ion chamber dosimetry[4] is

$$D_{\rm water}=MN_{\rm gas}(\overline{L}/\rho)^{\rm water}_{\rm air}P_{\rm ion}P_{\rm repl}P_{\rm wall}, \tag{1}$$

where M is the electrometer reading, $N_{\rm gas}$ is the cavity-gas calibration factor which is a constant, and $P_{\rm ion}, P_{\rm repl}, P_{\rm wall}$ are ion recombination, replacement, and chamber wall correction factors, respectively, which may vary with beam conditions. $P_{\rm wall}$ is taken as unity for electron beams[4] and hence is constant. The value of $P_{\rm ion}$ does not change significantly with dose rate (and hence field size and depth in a phantom) when $P_{\rm ion}$ is close to unity,[5] although the size of the correction is proportional to the dose rate. However, if $P_{\rm ion}$ is not close to unity, which might happen with a high-dose rate pulsed-swept beam, halving the dose rate would reduce it significantly toward unity. If this is the case, ignoring $P_{\rm ion}$ variation could introduce a couple of percent overestimate of ROFs.

The water to air restricted mean mass collision stopping-power ratio, $(\overline{L}/\rho)^{\rm water}_{\rm air}$, is a function of depth in water.[1,4,6] As discussed below, our calculations show that it is also a function of field size. For electron beam relative output measurements, which are usually done at $d_{\rm max}$ for each beam, $P_{\rm repl}$ is unity if a well-guarded plane-parallel chamber is used.[4,7,8] For cylindrical or poorly guarded plane-parallel chambers, $P_{\rm repl}$ is also a function of depth in phantom.

Given the above variations in these parameters, the relative output factors (ROF) of beams with different field sizes defined by cutouts within a given applicator are deduced from measurements as:

$$\begin{aligned}{\rm ROF}(A)&=\frac{(D/U)(A,d_{\rm max})}{(D/U)(A_0,d_{\rm max0})}\\&=\frac{(M/U)(A,d_{\rm max})\cdot(\overline{L}/\rho)^{\rm water}_{\rm air}|_{A,d_{\rm max}}\cdot P_{\rm repl}|_{d_{\rm max}}}{(M/U)(A_0,d_{\rm max0})\cdot(\overline{L}/\rho)^{\rm water}_{\rm air}|_{A_0,d_{\rm max0}}\cdot P_{\rm repl}|_{d_{\rm max0}}},\end{aligned} \tag{2}$$

where D/U, M/U are dose and ionization reading per monitor unit, respectively, A is the field size defined by the cutout, and A_0 is the reference field size; we have ignored any varia-

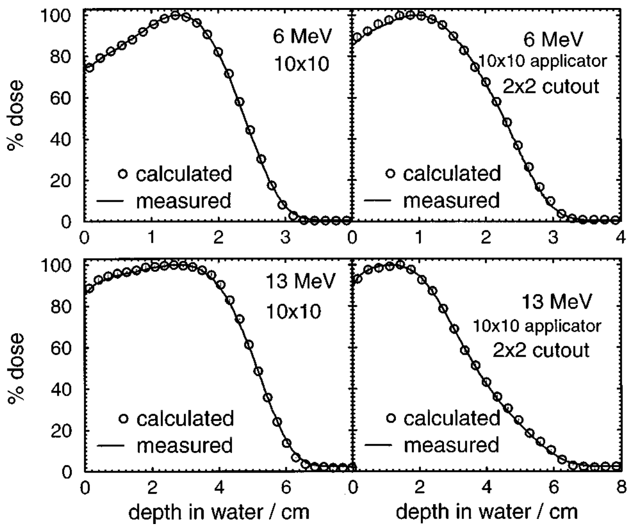

FIG. 1. Depth-dose curves of 6 and 13 MeV beams at SSD=100 cm. The measurements are done using a silicon diode detector. The Monte Carlo calculated curves agree with measurement very well. Significant $d_{\max}$ shifts are also shown.

tion in P_{ion} and polarity effects. It is well known that for small field sizes, the depth of dose maximum, $d_{\max}$, moves toward the surface. If one follows the recommendation of the AAPM's report on clinical electron beam dosimetry (TG-25, Khan *et al.*),[9] then in Eq. (2) one would take into account the variation of the stopping-power ratio and P_{repl} with depth as $d_{\max}$ changes.

For large fields, there is no $d_{\max}$ shift among depth-dose curves, i.e., $d_{\max}=d_{\max 0}$. The values of $(\bar{L}/\rho)^{\text{water}}_{\text{air}}$ and P_{repl} in Eq. (2) cancel out because they are not a function of field size in large beams. Thus the ROF for large beams can be calculated as the ratio of the two ionization readings per monitor unit, i.e.,

$$\text{ROF}(A)=\frac{(M/U)(A,d_{\max})}{(M/U)(A_0,d_{\max 0})}. \tag{3}$$

For small fields where $d_{\max}$ values shift significantly compared to that of a broad beam, the values of $(\bar{L}/\rho)^{\text{water}}_{\text{air}}$ at the corresponding $d_{\max}$ values are no longer the same. The value of P_{repl} may change with depth as well, but the variation in P_{repl} is small compared to that of $(\bar{L}/\rho)^{\text{water}}_{\text{air}}$. Nonetheless, it should be corrected for, if a cylindrical or poorly guarded plane-parallel chamber is used.

Based on the values of P_{repl} versus mean energy at depth given in TG-21, the effect of P_{repl} variation due to the $d_{\max}$ shift is up to about one-half percent change in ROFs for MD2 machines for an RK 83-05 chamber with an inner diameter of 4 mm. This effect is in the opposite direction of that due to the $(\bar{L}/\rho)^{\text{water}}_{\text{air}}$ change with depth. For a Farmer chamber with a 6.4 mm inner diameter the effect would be up to 1%. All measured values of P_{repl} are for broad beams.[4,10] Values for small beams are not known, thus in practice we assume they are the same as for broad beams.

If TG-25[9] is carefully followed in clinical practice, this $(\bar{L}/\rho)^{\text{water}}_{\text{air}}$ variation due to $d_{\max}$ shift is taken into account and Eq. (3) should not be used in ROF measurement for small fields.

Since TG-21 or TG-25 only give $(\bar{L}/\rho)^{\text{water}}_{\text{air}}|_{\infty,d_{\max}}$ for broad beams, the stopping-power ratio for the smaller field sizes, i.e., $(\bar{L}/\rho)^{\text{water}}_{\text{air}}|_{A,d_{\max}}$, is not available. Hence Eq. (2) cannot be applied in clinical practice. Instead, the ratio of $(\bar{L}/\rho)^{\text{water}}_{\text{air}}|_{\infty,d_{\max}}$ to $(\bar{L}/\rho)^{\text{water}}_{\text{air}}|_{\infty,d_{\max 0}}$ is used in Eq. (2) if TG-25 is carefully followed clinically. This paper will investigate how this approximation in TG-25 affects ROF measurements. Furthermore, the $(\bar{L}/\rho)^{\text{water}}_{\text{air}}$ data in TG-21 or TG-25 are for mono-energetic beams. In the real world, the beams from clinical accelerators are neither mono-energetic nor parallel. Values of $(\bar{L}/\rho)^{\text{water}}_{\text{air}}$ for the realistic beams from clinical accelerators differ by up to 1.4% from values for mono-energetic beams at $d_{\max}$ for broad beams.[11] In this paper we will use $(\bar{L}/\rho)^{\text{water}}_{\text{air}}$ data for realistic beams from Monte Carlo simulation and compare the results with those using TG-21 or TG-25 data.

For good clinical practice, one also needs to pay attention to other effects for small fields, such as the stem effect or polarity effect.[3,12] We will not discuss these effects in this paper.

II. SIMULATION/CALCULATION

We use BEAM,[13] an EGS4[14] user code, to simulate realistic clinical accelerator beams and the central-axis dose in a water phantom. Figure 1 presents two pairs of depth-dose curves for an MD2 accelerator to demonstrate that the agreement between the calculations and measurements is very good. It also shows the well known fact that $d_{\max}$ changes significantly for small field beams compared to a large field.

BEAM creates phase space files in which the energy, charge, position, and direction of every particle at the phantom surface are stored. We use these phase space files as inputs to the EGS4 user code SPRRZ[11,15,16] to calculate the realistic $(\bar{L}/\rho)^{\text{water}}_{\text{air}}$ curves. SPRRZ is also used to calculate $(\bar{L}/\rho)^{\text{water}}_{\text{air}}$ for mono-energetic beams. In these calculations, the $(\bar{L}/\rho)^{\text{water}}_{\text{air}}$ values are calculated for on-axis regions with 1 cm diameter to match the situation that a cylindrical chamber with a 1 cm long air cavity is used in the output measurements. All of the $(\bar{L}/\rho)^{\text{water}}_{\text{air}}$ calculations are based on the stopping powers of ICRU Report 37,[17] and $\Delta=10$ keV. The statistical uncertainty (1σ) on the $(\bar{L}/\rho)^{\text{water}}_{\text{air}}$ calculations is 0.1% or less.

III. RESULTS

A. Variations of stopping-power ratios

Figure 2 shows calculated stopping-power ratios versus depth for both mono-energetic and realistic beams. Figure 2(d) presents a comparison of $(\bar{L}/\rho)^{\text{water}}_{\text{air}}$ versus depth for broad mono-energetic beams of 6 MeV electrons as calculated here and as given in TG-21 or TG-25. The agreement is excellent except near the surface where Malamut *et al.* pointed out that the calculations in TG-21 have some

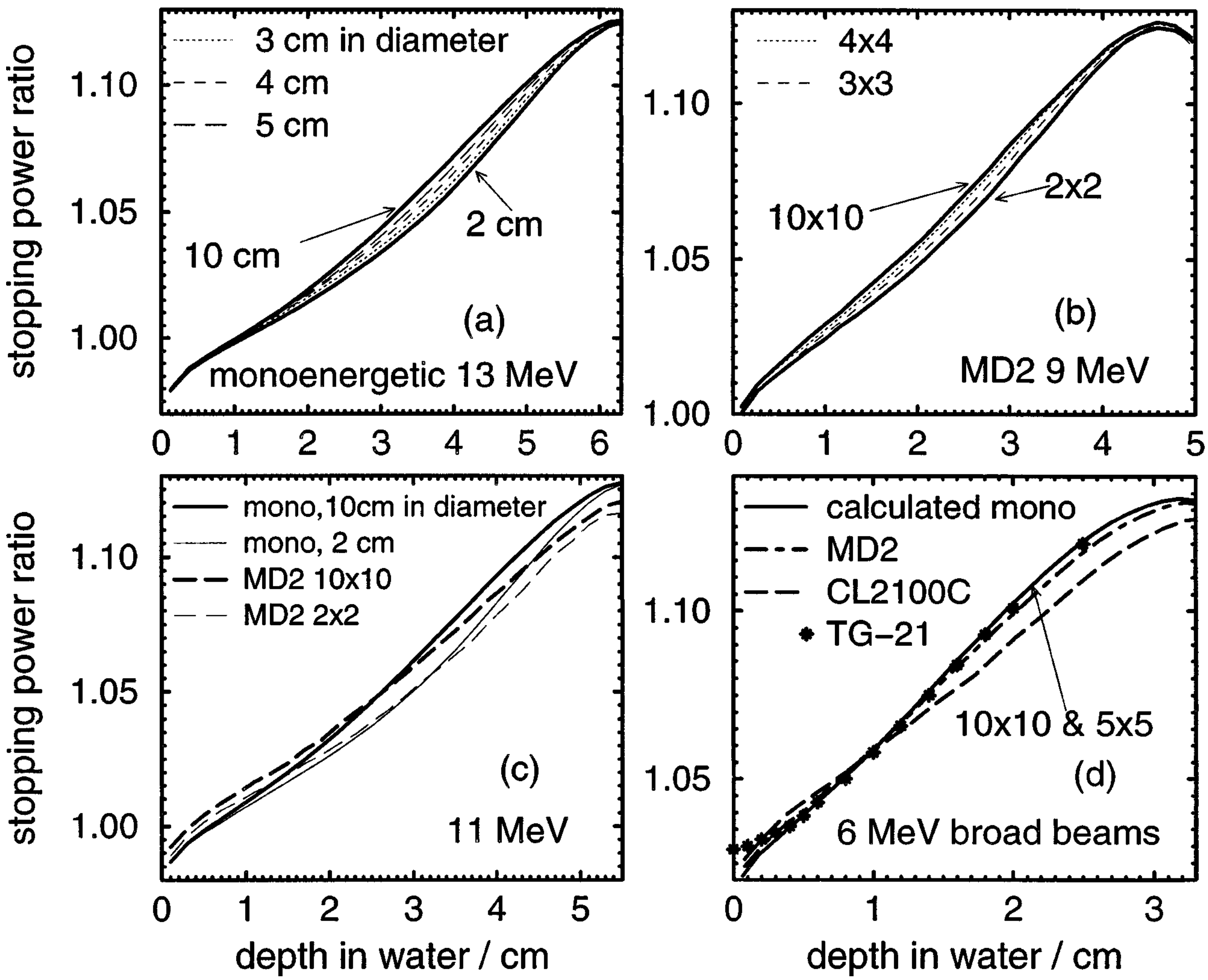

FIG. 2. $(\overline{L}/\rho)^{\text{water}}_{\text{air}}$ versus depth curves (a) for 13 MeV mono-energetic parallel beams of various field sizes incident on a water phantom; (b) for 9 MeV realistic MD2 beams for various cutout sizes; (c) for 11 MeV mono-energetic and realistic MD2 broad and narrow beams; (d) for different broad beams of 6 MeV electrons.

approximations.[15] The calculated realistic $(\overline{L}/\rho)^{\text{water}}_{\text{air}}$ data for broad 6 MeV beams are also compared in this figure.

Our calculations show that stopping-power ratios are a function of the beam field size. In Fig. 2(a), stopping-power ratios versus depth are presented for different field sizes for 13 MeV mono-energetic parallel beams. The values of stopping-power ratio at a given depth for small fields are lower than those for large fields. For example, at $d_{\max}$ in the $10\times 10\ \text{cm}^2$ beam (at 2.9 cm), the stopping-power ratio decreases by about 1% as the beam size decreases to a $2\times 2\ \text{cm}^2$ field. At $d_{\max}$ in the $2\times 2\ \text{cm}^2$ beam (at 1.3 cm), the difference of $(\overline{L}/\rho)^{\text{water}}_{\text{air}}$ values between $10\times 10\ \text{cm}^2$ and $2\times 2\ \text{cm}^2$ fields is only 0.2% since the curves are not spread out at this depth. Figure 2(b) shows that stopping-power ratio curves for realistic beams also differ with field size, although in this case slightly less than in the above mono-energetic case. The reason for the decrease with field size is that the low energy electrons are easily scattered away from the central axis and a corresponding number are not scattered in for small fields, thus the mean energy of the beam close to the central axis for a small field is larger than that of a large beam at a given depth, which corresponds to a smaller $(\overline{L}/\rho)^{\text{water}}_{\text{air}}$ value for a small field than that of a large field at that depth. At the phantom surface, the mean energy is about the same for different field sizes (for mono-energetic beams, it is exactly the same) and hence the $(\overline{L}/\rho)^{\text{water}}_{\text{air}}$ curves for different field sizes are the same at the phantom surface. Figure 2(c) compares the curves for 11 MeV mono-energetic and realistic beams. The curves for mono-energetic beams always have larger slopes than those of realistic beams.[11]

The following observations can be drawn from Fig. 2.

The maximum difference between stopping-power ratios for realistic beams and mono-energetic beams is more significant at higher energies for a given accelerator [compare Fig. 2(c) with Fig. 2(d) for MD2 curves], although at $d_{\max}$, it depends on the position of $d_{\max}$ relative to the crossover point of $(\overline{L}/\rho)^{\text{water}}_{\text{air}}$ versus depth for mono-energetic and realistic beams. The difference between the curves with different field sizes is also energy dependent. At 6 MeV, the stopping-power ratio curve for the beam defined by a 5

TABLE I. Corrections needed for MD2 ROFs for small cutout sizes measured without accounting for changes in $(\overline{L}/\rho)^{\text{water}}_{\text{air}}$ with depth [Eq. (3)]. Values of $f^{\text{mono}}_{\text{broad}}$ and $f^{\text{realistic}}_{\text{broad}}$ are for the broad beam method based on TG-21 (or TG-25) and realistic beam data, respectively, $f^{\text{mono}}_{\text{f.s.}}$ and $f^{\text{realistic}}_{\text{f.s.}}$ are for the field-size dependent method based on calculated mono-energetic data and realistic accelerator beam data, respectively.

Energy	13 MeV					9 MeV			
Cutout/cm^2	2×2	3×3	4×4	5×5	10×10	2×2	3×3	4×4	10×10
d_{max} /cm	1.3	2.0	2.5	2.7	2.9	1.1	1.7	2.0	2.1
$f^{\text{mono}}_{\text{broad}}$	0.965	0.979	0.990	0.995	-	0.968	0.987	0.997	-
$f^{\text{realistic}}_{\text{broad}}$	0.970	0.983	0.992	0.996	-	0.975	0.990	0.997	-
$f^{\text{mono}}_{\text{f.s.}}$	0.963	0.976	0.987	0.993	-	0.965	0.983	0.994	-
$f^{\text{realistic}}_{\text{f.s.}}$	0.967	0.979	0.989	0.994	-	0.972	0.986	0.996	-
Energy	11 MeV					6 MeV			
Cutout/cm^2	2×2	3×3	4×4	5×5	10×10	2×2	3×3	4×4	10×10
d_{max} /cm	1.2	1.95	2.25	2.45	2.6	1.0	1.25	1.4	1.45
$f^{\text{mono}}_{\text{broad}}$	0.966	0.983	0.990	0.996	-	0.982	0.992	0.998	-
$f^{\text{realistic}}_{\text{broad}}$	0.971	0.985	0.992	0.997	-	0.983	0.992	0.998	-
$f^{\text{mono}}_{\text{f.s.}}$	0.963	0.979	0.987	0.994	-	0.977	0.989	0.997	-
$f^{\text{realistic}}_{\text{f.s.}}$	0.967	0.983	0.988	0.996	-	0.978	0.989	0.998	-

$\times 5\ \text{cm}^2$ cutout is identical to that of the broad beam [Fig. 2(d)] while for the 13 MeV case there is an obvious difference [Fig. 2(a)]. At d_{max} for small beams, the difference is larger for lower energies since for low energy beams, curves of $(\overline{L}/\rho)^{\text{water}}_{\text{air}}$ versus depth are well spread out at d_{max} for small fields while for high energy beams they are not. The slope of a stopping-power ratio curve also varies with energy, the higher the energy, the smaller the slope.

B. Corrections to relative output factors

Since d_{max} moves upstream for small fields, $(\overline{L}/\rho)^{\text{water}}_{\text{air}}$ values decrease and thus ROFs for small fields are overestimated using Eq. (3) instead of Eq. (2). To measure ROFs accurately, proper values of $(\overline{L}/\rho)^{\text{water}}_{\text{air}}$ for the corresponding depth and field size should be used. To correct Eq. (3) completely for the effects of changes in $(\overline{L}/\rho)^{\text{water}}_{\text{air}}$ one needs

$$f_{\text{f.s.}}=\frac{(\overline{L}/\rho)^{\text{water}}_{\text{air}}|_{A,d_{\text{max}}}}{(\overline{L}/\rho)^{\text{water}}_{\text{air}}|_{A_0,d_{\text{max0}}}}. \tag{4}$$

This is the field-size (f.s.) dependent correction method in which values of $(\overline{L}/\rho)^{\text{water}}_{\text{air}}$ from curves for different field sizes are used.

The above correction is accurate but it requires knowing $(\overline{L}/\rho)^{\text{water}}_{\text{air}}$ as a function of field size for each accelerator beam. This makes the correction complicated. Clinically, it is not practical. A simple approach is to use just broad beam data:

$$f_{\text{broad}}=\frac{(\overline{L}/\rho)^{\text{water}}_{\text{air}}|_{\infty,d_{\text{max}}}}{(\overline{L}/\rho)^{\text{water}}_{\text{air}}|_{\infty,d_{\text{max0}}}}. \tag{5}$$

The $(\overline{L}/\rho)^{\text{water}}_{\text{air}}$ data for mono-energetic broad beams are given in TG-21 or TG-25.

We have calculated $f_{\text{f.s.}}$ for open applicators using $(\overline{L}/\rho)^{\text{water}}_{\text{air}}$ values for realistic MD2 beams. These correction are within 1% of unity for the smallest applicator (5 cm diameter), even at the higher energies, and are not needed for other applicators because d_{max} does not shift significantly for open applicators and there is little field-size dependence.

In contrast, it is well known that the d_{max} shifts are significant for small fields defined by cutouts.[9] Based on the d_{max} data measured by Cygler *et al.*,[18] Table I presents corrections based on the different $(\overline{L}/\rho)^{\text{water}}_{\text{air}}$ data and methods. To specify TG-21 or TG-25 $(\overline{L}/\rho)^{\text{water}}_{\text{air}}$ values the mean incident energy is calculated based on Rogers and Bielajew's specification of electron beam energy[19] and linear interpolation is applied to the tabulated values. The $(\overline{L}/\rho)^{\text{water}}_{\text{air}}$ change due to the d_{max} shift is insensitive to the details of the energy which is selected for the TG-21 or TG-25 data. The factors $f^{\text{mono}}_{\text{broad}}$ and $f^{\text{realistic}}_{\text{broad}}$ are based on the broad beam method, with $(\overline{L}/\rho)^{\text{water}}_{\text{air}}$ data from TG-21 or TG-25 and from realistic MD2 beams, respectively. The factors $f^{\text{mono}}_{\text{f.s.}}$ and $f^{\text{realistic}}_{\text{f.s.}}$ are based on the field-size dependent method, with mono-energetic and realistic beam data, respectively.

The factor $f^{\text{mono}}_{\text{broad}}$, which is the factor used if TG-25 is followed, is about 3% less than unity for $2\times 2\ \text{cm}^2$ fields for all energies except 6 MeV (Table I). This means that if Eq. (3) is used in ROF measurements for small fields, the ROFs are overestimated by up to 3% based on the $(\overline{L}/\rho)^{\text{water}}_{\text{air}}$ data from TG-25. However, the factor $f^{\text{mono}}_{\text{broad}}$ does not take into account the effect of field size on stopping-power ratio and ignores the difference in $(\overline{L}/\rho)^{\text{water}}_{\text{air}}$ between realistic and mono-energetic beams.

To take into account the field-size effect on stopping-power ratio, the factor $f^{\text{mono}}_{\text{f.s.}}$ is calculated for different field sizes and energies. This factor still uses stopping-power ratio data for mono-energetic beams. The factor is a few tenths percent (up to 0.5%) smaller than the factor $f_{\rm broad}^{\rm mono}$ which means the correction is up to 0.5% larger. This is the size of the difference of $(\bar{L}/\rho)_{\rm air}^{\rm water}$ values between the field size of interest and the reference field at the $d_{\rm max}$ of the field of interest (which tends to be larger at lower energies).

The factor $f_{\rm broad}^{\rm realistic}$ is the same as $f_{\rm broad}^{\rm mono}$ but uses $(\bar{L}/\rho)_{\rm air}^{\rm water}$ values for incident realistic broad beams instead of the stopping-power ratio data from TG-21 or TG-25 for incident mono-energetic beams. Since the slope of a broad mono-energetic $(\bar{L}/\rho)_{\rm air}^{\rm water}$ data curve is always higher than that of a curve for a realistic beam with the same mean energy, values of $f_{\rm broad}^{\rm mono}$ in Table I are always smaller than $f_{\rm broad}^{\rm realistic}$ for small fields by up to 0.7%, i.e., the implied corrections are smaller for $f_{\rm broad}^{\rm realistic}$ by up 0.7% compared to $f_{\rm broad}^{\rm mono}$.

Considering both the field-size effect on stopping-power ratio and using stopping-power ratio data for realistic beams, we calculate the factor $f_{\rm f.s.}^{\rm realistic}$. In Table I, the values of factors $f_{\rm broad}^{\rm mono}$ and $f_{\rm f.s.}^{\rm realistic}$ are very close for every field size for a given energy. The analysis of factors $f_{\rm f.s.}^{\rm mono}$ and $f_{\rm broad}^{\rm realistic}$ above shows that the field-size effect and the difference between using realistic and mono-energetic stopping-power ratio data are in the opposite directions for the correction factors, thus tend to cancel each other in factor $f_{\rm f.s.}^{\rm realistic}$. In principle, using $f_{\rm f.s.}^{\rm realistic}$ is the most accurate correction. Our calculations show that the difference between $f_{\rm broad}^{\rm mono}$ and $f_{\rm f.s.}^{\rm realistic}$ is no more than 0.4%, which means, from the view of clinical practice, following TG-25, i.e., using $f_{\rm broad}^{\rm mono}$, will correct the error due to using Eq. (3) in the ROF measurement to within 0.4%.

In the example of $(\bar{L}/\rho)_{\rm air}^{\rm water}$ versus depth for Varian Clinac 2100C accelerator [Fig. 2(d)], the difference between the values of $(\bar{L}/\rho)_{\rm air}^{\rm water}$ for realistic and mono-energetic beams at $d_{\rm max}$ in a $10\times10\ {\rm cm}^2$ field is well compensated by the difference between the $(\bar{L}/\rho)_{\rm air}^{\rm water}$ values for $10\times10\ {\rm cm}^2$ and $2\times2\ {\rm cm}^2$ fields at the $d_{\rm max}$ of the $2\times2\ {\rm cm}^2$ field (not shown in the figure). The difference between using $f_{\rm f.s.}^{\rm realistic}$ and $f_{\rm broad}^{\rm mono}$ is thus smaller than 0.4%, which is the difference for the same case but for the MD2 machine.

For other clinical accelerators which produce ''dirtier'' beams (which means more scattered component in the beams), the $d_{\rm max}$ shift is smaller compared to that of the MD2 machine which produces beams which are closer to mono-energetic beams. This is especially true for high energy beams. Although the difference of $(\bar{L}/\rho)_{\rm air}^{\rm water}$ between realistic and mono-energetic beams can be quite large at $d_{\rm max}$ for broad beams (up to 1.4%[11]), the change in the ratio of $(\bar{L}/\rho)_{\rm air}^{\rm water}$ for realistic versus mono-energetic beams with a small change in $d_{\rm max}$ is usually small. Considering the field-size effect on $(\bar{L}/\rho)_{\rm air}^{\rm water}$, which is in the opposite direction to the change in this ratio, the difference between using $f_{\rm f.s.}^{\rm realistic}$ and $f_{\rm broad}^{\rm mono}$ is not expected to be significantly worse than the results for the MD2 machine.

Burns *et al.*[20] gave a function which calculates $(\bar{L}/\rho)_{\rm air}^{\rm water}$ values for $10\times10\ {\rm cm}^2$ realistic beams as a function of R_{50} over a large range of depths in a water phantom. Using $(\bar{L}/\rho)_{\rm air}^{\rm water}$ values from this function (available at http://www.irs.inms.nrc.ca/inms/papers/SPRR50/sprR50.html) gives a result similar to $f_{\rm broad}^{\rm realistic}$ (less than 0.3% difference). Since this differs more from the values of $f_{\rm f.s.}^{\rm realistic}$ than $f_{\rm broad}^{\rm mono}$, there is nothing gained from using this more accurate function for broad beams in this application.

IV. SUMMARY AND CONCLUSIONS

We have confirmed that when measuring ROFs for small field sizes using ion chambers, considerable care must be taken to follow TG-25, i.e., ensure that variations in the values of $(\bar{L}/\rho)_{\rm air}^{\rm water}$ and other factors are taken into account. Ignoring the variation in $(\bar{L}/\rho)_{\rm air}^{\rm water}$ due to the change of depth of the measurement point as the field size gets smaller can lead to overestimates of the ROF by up to 3%.

We have shown that the stopping-power ratio is a function of field size. Ignoring this effect leads to errors in ROF of up to one-half percent for small fields.

Values of stopping-power ratio also vary with accelerator. Using stopping-power ratio data for mono-energetic beams, instead of those for realistic beams, introduces an error in ROF of up to 0.7% for small fields but in the opposite direction of the field-size effect.

Since the error from using stopping-power ratio data for broad beams and the error from using stopping-power ratio data for mono-energetic instead of realistic beams tend to cancel each other, following TG-25 will give an ROF result for a MD2 machine which is accurate within 0.4% for small fields. Due to the smaller $d_{\rm max}$ shift for other accelerators with beams which are less mono-energetic, this upper estimate of the error in using the mono-energetic broad beam data will still be correct.

ACKNOWLEDGMENTS

We would like to thank Jan Seuntjens, Iwan Kawrakow, Ken Shortt, Blake Walters, Daryoush Sheikh-Bagheri, Miller MacPherson, and Michel Proulx, all at NRC, for helpful discussions and computer system support. We thank George Ding of the Fraser Valley Cancer Centre, and Charlie Ma of Stanford University for helpful discussions.

[a]Electronic-mail: dave@irs.phy.nrc.ca; WWW: http://www.irs.inms.nrc.ca/inms/irs/papers/irs_www/irs_www.html.

[1]A. Niroomand-Rad, M. T. Gillin, R. W. Kline, and D. F. Grimm, ''Film dosimetry of small electron beams for routine radiotherapy planning,'' Med. Phys. **13**, 416–421 (1986).

[2]A. Niroomand-Rad, ''Film dosimetry of small elongated electron beams for treatment planning,'' Med. Phys. **16**, 655–662 (1989).

[3]G. G. Zhang, D. W. O. Rogers, J. E. Cygler, and T. R. Mackie, ''Monte Carlo calculated electron beam output factors vs cutout size,'' Med. Phys. (submitted).

[4]AAPM TG-21, ''A protocol for the determination of absorbed dose from high-energy photon and electron beams,'' Med. Phys. **10**, 741–771 (1983).

[5]J. M. Havercroft and S. C. Klevenhagen, ''Ion recombination corrections for plane-parallel and thimble chambers in electron and photon radiation,'' Phys. Med. Biol. **38**, 25–38 (1993).

[6]IAEA, *Absorbed Dose Determination in Photon and Electron Beams; An International Code of Practice*, Vol. 277 of Technical Report Series (IAEA, Vienna, 1987).

[7]P. R. Almond, F. H. Attix, S. Goetsch, L. J. Humphries, H. Kubo, R. Nath, and D. W. O. Rogers, ''The calibration and use of plane-parallel

ionization chambers for dosimetry of electron beams: An extension of the 1983 AAPM protocol, Report of AAPM Radiation Therapy Committee Task Group 39,'' Med. Phys. **21**, 1251–1260 (1994).

[8]A. Van der Plaetsen, J. Seuntjens, H. Thierens, and S. Vynckier, ''Verification of absorbed doses determined with thimble and parallel-plate ionization chambers in clinical electron beams using ferrous sulphate dosimetry,'' Med. Phys. **21**, 37–44 (1994).

[9]F. M. Khan, K. P. Doppke, K. R. Hogstrom, G. J. Kutcher, R. Nath, S. C. Prasad, J. A. Purdy, M. Rozenfeld, and B. L. Werner, ''Clinical electron-beam dosimetry: Report of AAPM Radiation Therapy Committee Task Group 25,'' Med. Phys. **18**, 73–109 (1991).

[10]K. A. Johansson, L. O. Mattsson, L. Lindborg, and H. Svensson, ''Absorbed-dose determination with ionization chambers in electron and photon beams having energies between 1 and 50 MeV,'' IAEA Symposium Proceedings (Vienna) IAEA-SM-222/35, pp. 243–270 (1977).

[11]G. X. Ding, D. W. O. Rogers, and T. R. Mackie, ''Calculation of stopping-power ratios using realistic clinical electron beams,'' Med. Phys. **22**, 489–501 (1995).

[12]H. Aget and J. C. Rosenwald, ''Polarity effect for various ionization chambers with multiple irradiation conditions in electron beams,'' Med. Phys. **18**, 67–72 (1991).

[13]D. W. O. Rogers, B. A. Faddegon, G. X. Ding, C. M. Ma, J. Wei, and T. R. Mackie, ''BEAM: A Monte Carlo code to simulate radiotherapy treatment units,'' Med. Phys. **22**, 503–524 (1995).

[14]W. R. Nelson, H. Hirayama, and D. W. O. Rogers, ''The EGS4 Code System,'' Report SLAC-265, Stanford Linear Accelerator Center, Stanford, CA (1985).

[15]C. Malamut, D. W. O. Rogers, and A. F. Bielajew, ''Calculation of water/air stopping-power ratios using EGS4 with explicit treatment of electron—positron differences,'' Med. Phys. **18**, 1222–1228 (1991).

[16]A. Kosunen and D. W. O. Rogers, ''Beam quality specification for photon beam dosimetry,'' Med. Phys. **20**, 1181–1188 (1993).

[17]ICRU, ''Stopping powers for electrons and positrons,'' ICRU Report 37, ICRU, Washington D.C. (1984).

[18]J. Cygler, X. A. Li, G. X. Ding, and E. Lawrence, ''Practical approach to electron beam dosimetry at extended SSD,'' Phys. Med. Biol. **42**, 1505–1514 (1997).

[19]D. W. O. Rogers and A. F. Bielajew, ''Differences in electron depth dose curves calculated with EGS and ETRAN and improved energy range relationships,'' Med. Phys. **13**, 687–694 (1986).

[20]D. T. Burns, G. X. Ding, and D. W. O. Rogers, ''R_{50} as a beam quality specifier for selecting stopping-power ratios and reference depths for electron dosimetry,'' Med. Phys. **23**, 383–388 (1996).